Evaluation of the self-healing capacity of ceramics produced with alumina and silicon carbide

N. R. de Souza[1]*, P. R. P. de Paiva[1]

[1]Centro Federal de Educação Tecnológica de Minas Gerais, Departamento de Engenharia de Materiais, Belo Horizonte, MG, Brazil

Abstract

The self-healing capacity of a ceramic material produced by uniaxial pressing with alumina (Al_2O_3), silicon carbide (SiC), and magnesium oxide (MgO) was evaluated. To assess self-healing, a discontinuity was generated on the surface of the specimens. The healing time in the oven, at a temperature of 1000 ºC, was 1, 30, and 60 min. The specimens were analyzed by physical and mechanical tests. The results showed that, for the mixture containing 15% SiC, the specimens healed at 60 min had an increase in flexural strength of 84.9% when compared to the specimens that were only indented while for the specimens containing 20% SiC, this increase was 61.1% at 30 min. For the 30 min healing time, there was a reduction in the size of the discontinuity in the specimens by about 19.1% and 14.8%, for the formulation containing 15% and 20% of SiC, respectively.

Keywords: self-healing, alumina, silicon carbide, activating agent.

INTRODUCTION

Self-healing materials are a new class of intelligent materials that can partially or fully recover their mechanical properties after the appearance of a defect (mainly cracks), due to their use [1]. These materials have the ability to recover functionality autonomously or externally assisted, and the restoration of their properties depends mainly on the choice of healing agents [2-4]. They can be obtained from different classes of materials with different intrinsic properties because in all classes the self-healing procedure uses the same underlying concepts and is based on the same general principle [1]. The probable recovery of mechanical properties is due to the formation of a mobile phase since this phase reacts with the surface of the defect and this reaction allows the reconnection of the planes by physical interactions and/or chemical bonds. After healing, the discontinuity is immobilized, resulting in the restoration of most of the mechanical properties [1]. The self-healing property also allows these materials to be used to protect or reduce oxidation or corrosion, as a self-healing protective coating, or even to improve mechanical properties [5-7]. The self-healing process would be a great advance in the use of ceramic materials, since it is known that the mechanical properties of these materials limit their use in some applications because they are subject to catastrophic fractures in a fragile way, with little energy absorption [8]. Therefore, studies have been carried out to create a ceramic material with the capacity of self-healing, and so providing a longer useful life and, consequently, an increase in the applicability of advanced ceramics [2, 8]. This technology can also become economically viable, since the self-healing process would reduce the replacement and exchange of parts with some superficial defect, influencing its functionality. Another relevant factor is that the self-healing procedure can be done *in situ*, thereby reducing downtime for replacing or repairing damaged parts [1].

Among the ceramic matrices that are being evaluated as self-healing, it is possible to mention the matrices produced with alumina (using silicon carbide as a healing agent) and carbon matrices (using silicon carbide or aluminum fibers as a healing agent), and it is worth mentioning that all the raw materials of the consulted studies are on a nanometric scale [9]. Currently, the research for ceramic materials with the self-healing property has focused on using silicon carbide as a healing agent in an alumina matrix, due to its stability, high specific volume when decomposed into oxide, and because it binds easily to the matrix [10]. Previous studies have shown that the addition of silicon carbide to alumina matrices improves the mechanical properties of the ceramic part, such as mechanical strength and wear resistance [11]. The self-healing process in ceramic materials is mainly induced by passive oxidation of the region containing the defect (crack). A determining factor for healing ceramic pieces is that the oxidation reaction only occurs at high temperatures [12]. Ando et al. [13] evaluated the self-healing feature of ceramic matrices produced based on alumina; silicon carbide was used as the healing agent. The self-healing property was demonstrated and reported as the consequence of the oxidation of silicon carbide when oxygen penetrated the cracks. The oxidation occurred under high temperatures and the material showed a high fatigue limit at room temperature and also at 1100 ºC. Chlup et al. [14] used a matrix produced with alumina and added silicon carbide to act as a healing agent. The healing took place at 1300 ºC for 1 h. As a result, the ceramic piece showed high values of flexural strength

**naira.raquel@yahoo.com.br*
https://orcid.org/0000-0002-2842-1400

and Young's elastic modulus. The healing procedure used was considered sufficient to completely recover the original properties of the specimens. Osada et al. [15] evaluated the self-healing process and strength recovery in alumina matrices, containing silicon carbide as a healing agent and a healing activator. The study showed that adding the activating agent can increase the self-healing rate by more than 6,000 times.

Healing activators are oxides that accelerate the healing process, enabling efficient delivery of oxygen and incorporating an additional healing network. The amount and type of activator are chosen based on the desired application [15]. For ceramic materials, a self-healing procedure can be carried out by encapsulating the healing agent [3], expanding the phases present in the material [1], by transport channel (mobile phase) [1], by biological processes [16], or by electrochemical processes [17]. Self-healing ceramics are fully capable of replacing existing ceramics because they are less sensitive to fragile flaws and enable a wide range of applications, longer service life, and greater reliability; however, high cost is a limiting factor [1, 9, 15, 18]. Within this context, the aim of this paper was to produce, by uniaxial pressing, a ceramic matrix based on alumina, using silicon carbide as a healing agent and magnesium oxide as a healing activator working with micrometric granulometry materials. This type of production potentially reduces costs with raw materials and processing and facilitates obtaining ceramic pieces with the ability to self-healing, improving mechanical properties.

MATERIALS AND METHODS

Raw materials: the material under study was manufactured from alumina (Al_2O_3 powder, 99.9% pure, Alcoa) for the matrix, 15% w/w (A1) and 20% w/w (A2) of silicon carbide particles (SiC, 97% pure, Saint-Gobain Brasil) as a healing agent, and 3% w/w of magnesium oxide particles (MgO powder, 97% pure, Proquímicos) as healing activator. MgO was used as received. To adjust the grain size, the alumina and silicon carbide were ground in a planetary ball mill (Pulverisette 5/4, Fritsch). The polyvinyl acetate (PVA, Sigma Aldrich 80% hydrolysate) was used to produce a binder solution with a concentration of 10% w/w (10 g of PVA and 100 g of distilled water); for this purpose, a magnetic stirrer (C-MAG HS7, Ika) was used.

Processing and sintering: the samples were defined according to the proportions of the raw materials described in Table I and mixed using the planetary ball mill. Values of SiC addition of 15% and 20% w/w are found in the literature [13, 14, 19]. The silicon carbide contents used were based on the literature since the results obtained for the self-healing ability were effective. The specimens were manufactured with dimensions of approximately 60.0x20.5x11.0 mm by uniaxial cold pressing using a hydraulic press (SL12, Solab). For pressing, a load of $1.2x10^8$ N/m^2 for 1 min was used. It should be emphasized that the use of this pressing methodology was determined experimentally. After preparation, the specimens were dried in an oven at 150 ºC for 24 h and sintered in an electric oven, without a controlled atmosphere, at 1400 ºC for 5 min [20]. The heating rate was 5 °C/min. 50 specimens were produced for each formulation. Of these 50, 10 were selected to be evaluated as sintered, 10 as indented, 10 after 1 min healing time, 10 after 30 min healing time, and 10 after 60 min healing time.

Table I - Formulation (mass fraction) of specimens.

Sample	SiC	Al_2O_3	MgO	Binder (PVA)
A1	15%	76%	3%	6%
A2	20%	71%	3%	6%

Methods of characterization: the analysis of the particle size distribution of the raw materials was performed by laser granulometry using a granulometer (mod. 1090, Cilas), making use of the Fraunhofer theory; the ultrasound time of the suspension, before the test, was 5 min using an obscuration index of 1%. The semiquantitative chemical composition of the raw materials was obtained by X-ray fluorescence (XRF) using a spectrometer (EDX-720, Shimadzu) under a vacuum. To carry out the analysis, the samples were pressed in the form of tablets with boric acid (H_3BO_3). The phases present in the raw materials and the specimens were identified by the powder method using a diffractometer (XRD 700, Shimadzu) under the following operating conditions: CuKα radiation (35 kV/40 mA), goniometer speed of 0.02° (2θ) per step, time counting of 1 s/step, and collected from 5° to 80° in 2θ. The interpretations of the XRD patterns were made by comparison with standards contained in the PDF 02 database [21]. We emphasize that X-ray fluorescence and X-ray diffraction were tools used to evaluate the purity of the samples. Linear shrinkage was performed to evaluate the influence of SiC addition on the sintering process. To calculate the shrinkage, the specimen dimensions were measured before and after sintering. The measurement was performed using a digital caliper (Mitutoyo) with a resolution of ±0.01 mm.

The self-healing feature evaluation was performed by comparing the physical and mechanical properties of the specimens, with or without discontinuity, and before and after the healing stage. The self-healing feature was also assessed by comparing the measure of the discontinuity size before the healing step and after the healing step. The discontinuity was made by a Vickers durometer (VEB Werkstoffprüfmaschinen Leipzig) with diamond penetrator, applying a load of 20 kgf for 15 s. Then the specimens were visualized with an optical microscope (PZO-Labimex, Metrimpex). The indentation measurements were obtained digitally using images taken under the microscope. The diagonals were measured and the average was taken, being the result of the discontinuity size exemplified in Fig. 1. After the generation of the discontinuity, some specimens were taken to the muffle furnace at 1000 °C with a holding time of 1, 30, and 60 min. The heating rate was 3 °C/min.

The healing temperature was kept fixed, varying only the time, being shorter than the healing time of other studies [13-15]. After the healing time, the samples were viewed again with an optical microscope to measure the discontinuities. The apparent porosity and water absorption tests from samples were determined by the ASTM C373-88 [22]. According to this standard, the specimens were weighed and then submerged in boiling water for a period of 3 h and cooled in water for 24 h. After cooling, the specimens were removed from the water, excess surface water was removed with the use of paper towels, and they were weighed again. The immersed weights were also obtained with the aid of a system in which the sample was immersed in water. For the mechanical test, the three-point bending test was used, which was carried out at room temperature using a universal mechanical testing machine (Autograph AG-X, Shimadzu), with a maximum load of 10 kN. The loading speed was 2 mm/min. The bending stress was calculated using the ABNT/NBR 13818:1997 standard [23] for each sample. All the microstructure observations were done by scanning electron microscopy (SEM, SSX-550, Shimadzu). For this purpose, the samples were covered with gold film by sputtering using a metallizer (Quick Coater SC-701, Sanyu Electron) and affixed to the sample holder with a carbon tape.

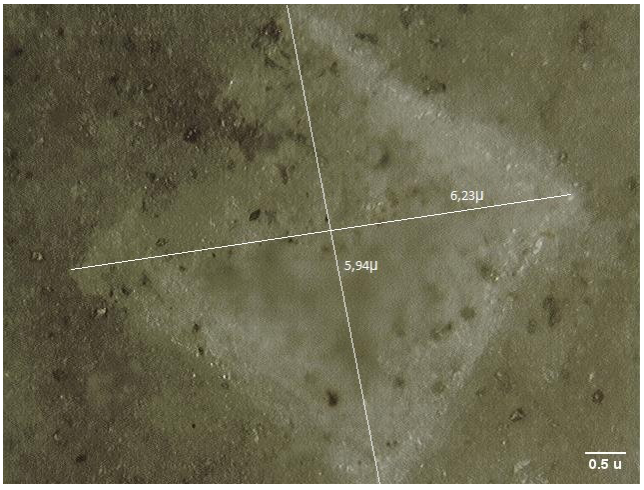

Figure 1: Image showing a discontinuity generated on the surface of the Al_2O_3/SiC ceramic sample.

RESULTS AND DISCUSSION

Characterization of raw materials: in Table II and Fig. 2, it is possible to observe that the average particle diameter of alumina was 7.39 µm, of silicon carbide was 5.60 µm, and that of magnesium oxide was 6.49 µm. The reductions in the particle size by the planetary mill of the alumina and silicon carbide powders were approximately 92.3% and 90.7%, respectively. Although in the literature some authors [13-15] worked with powders with nanometric granulometry, this research used the micrometric granulometry values obtained in order to minimize the cost of grinding the raw materials. In addition, it was observed that with a grinding time of more than 2 h, the alumina particles were agglomerating, a procedure that could hinder their dispersion during the production process of the specimens. The result of the semiquantitative chemical analysis can be seen in Table III. The powder samples were highly pure, as they contained high levels of aluminum oxide (99.6%), silicon oxide (97.6%; here Si content in SiC was expressed as oxide content), and magnesium oxide (93.7%) in the samples of alumina, silicon carbide, and magnesium oxide, respectively. The XRF results for the magnesium oxide sample had acceptable contents for SiO_2, CaO, and SO_3 impurities [24]. The XRD results for the samples of alumina, silicon carbide, and magnesium oxide can be seen in Fig. 3. The results for alumina (Fig. 3a) showed that the sample had basically an alumina phase in its composition (PDF-2 74-1081), with sodium and aluminum oxide (PDF-2 32-1033) as an impurity that may be correlated to the alumina production process [25]. This result corresponded with the study by Sarker et al. [26]. The diffractogram of the silicon carbide shown in Fig. 3b was compared with literature and tabulated standards for the silicon carbide phase (PDF-2 73-1407), showing only that phase. It was not possible to differentiate the α and β phases of SiC due to the reflections of the α phase overlapping those of the β phase, making it difficult to distinguish them [27]. The diffractogram of the MgO sample in Fig. 3c was also compared with tabulated standards and literature, showing that the sample was basically composed of the magnesium oxide (PDF-2 75-0447) and hydrated magnesium oxide (PDF-2 44-1482) phases. The presence of the hydrated magnesium oxide phase was probably due to MgO having a highly hygroscopic reaction with humidity in the environment [24, 28]. The results obtained by XRD for raw materials corroborated the results obtained by XRF,

Table II - Results of the granulometric analysis (µm) of the raw materials.

Raw material	D10	D50	D90	$D_{average}$
Al_2O_3	1.11	3.63	20.34	7.39
SiC	0.28	3.33	14.57	5.60
MgO	1.94	4.99	13.29	6.49

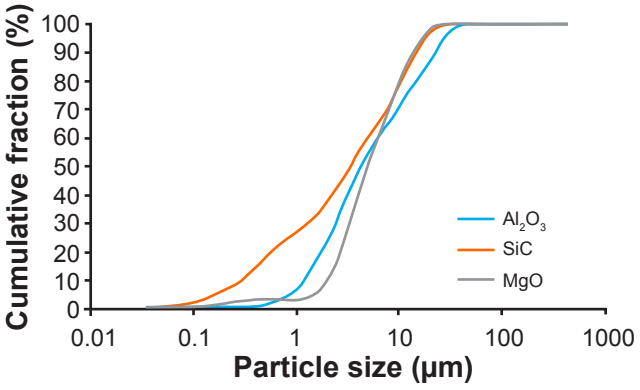

Figure 2: Particle size distribution curves of raw materials.

Table III - Results of semi-quantitative chemical analysis (wt%) by XRF of raw materials.

Sample	Al_2O_3	SiO_2	Fe_2O_3	MgO	CaO	SO_3	Others
Al_2O_3	99.6	-	-	-	-	-	0.4
SiC*	2.2	97.6	0.1	-	-	-	0.1
MgO	-	1.1	-	93.7	3.3	1.2	0.7

** results expressed as oxide contents.*

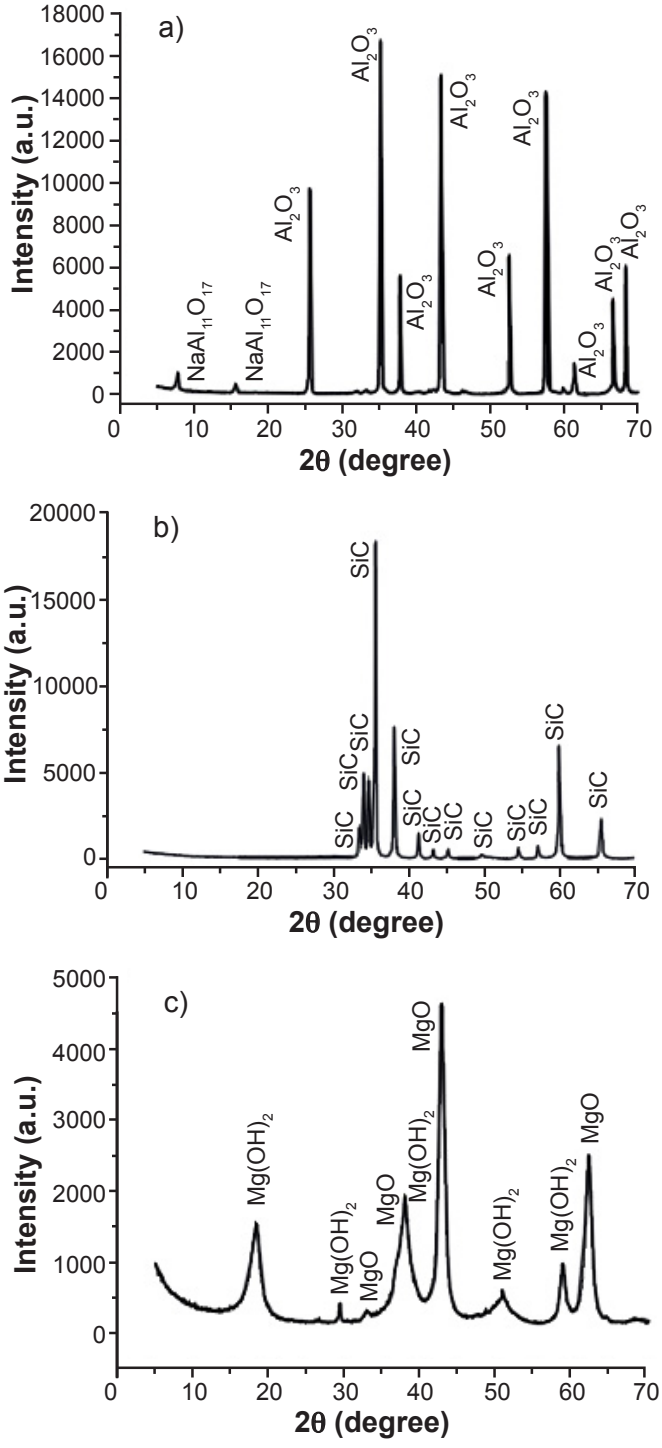

Figure 3: X-ray diffractograms of raw powders: a) alumina; b) silicon carbide; and c) magnesium oxide.

confirming the high degree of purity of the samples used for the production of the specimens.

Self-healing of ceramic samples: SEM images of the specimens are shown in Fig. 4. Analyzing the micrographs, it was seen that densification occurred in all samples. The micrograph of the A1 formulation had the highest coalescence index, indicating the best sinterability. It was observed that in sample A2 coalescence occurred, however less pronounced than in sample A1. Considering that strength is proportional to densification, it was expected that samples of formulation A2 had lower strength than the sample of formulation A1. The XRD results for the samples of both formulations can be seen in Fig. 5. The A1 formulation sample presented in its composition the phases Al_2O_3 (PDF-2 46-1212), SiC (PDF-2 75-0254), $Al_6Si_2O_{12}$ (PDF-2 74-2419), and $MgAl_2O_4$ (PDF-2 21-1152). The A2 formulation sample also had Al_2O_3 (PDF-2 71-1125), SiC (PDF-2 01-1119), $Al_6Si_2O_{12}$ (PDF-2 06-0258), and $MgAl_2O_4$ (PDF-2 11-1154) phases in its composition. From these results, it was evident that there was a phase containing silicon oxide present in each of the formulations. This phase was determined to be mullite, an aluminum silicate phase with the chemical formula $Al_6Si_2O_{12}$. As the amount of SiC increased, the intensity of Al_2O_3 decreased, which was expected. The addition of a curing activating agent also promoted the crystallization of

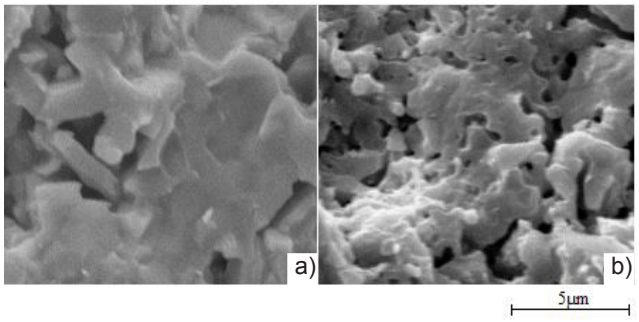

Figure 4: SEM images of sintered samples: a) A1 (15% SiC); and b) A2 (20% SiC).

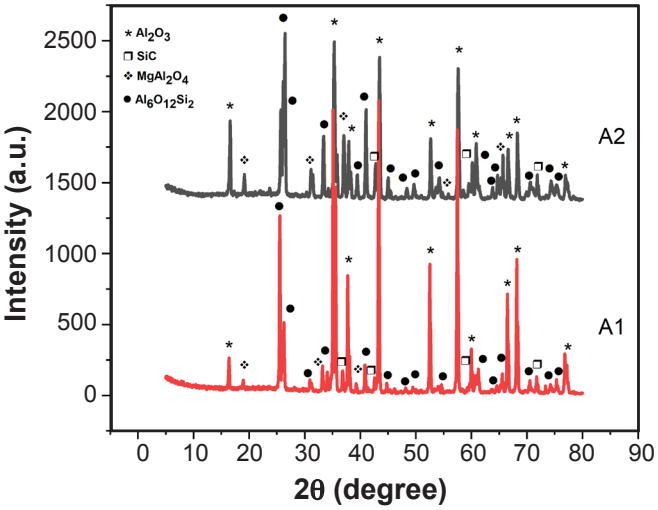

Figure 5: XRD patterns of the surface after healing of Al_2O_3/SiC ceramics doped with 3.0 wt% MgO.

Table IV - Results of linear shrinkage of sintered samples.

Sample	Shrinkage
A1	13.7%
A2	9.9%

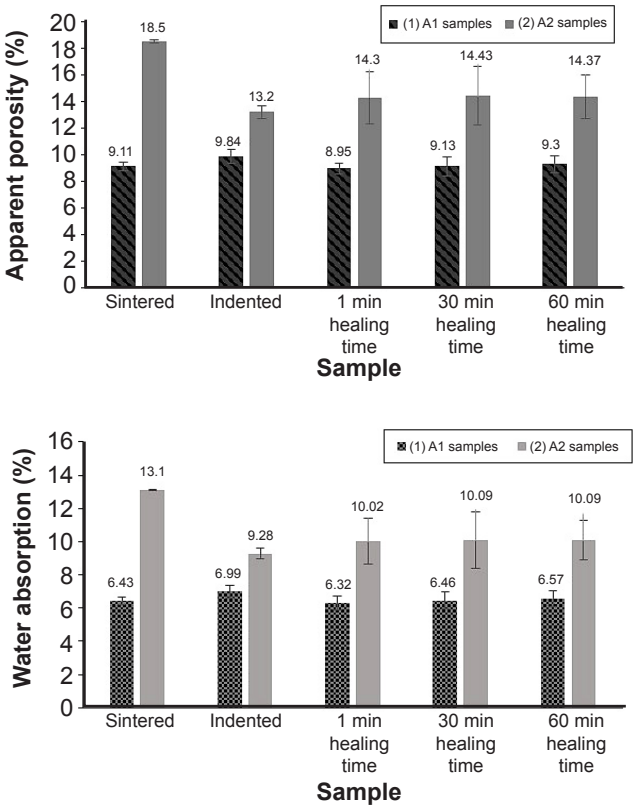

Figure 6: Apparent porosity (a) and water absorption (b) values of the samples A1 (15% SiC) and A2 (20% SiC).

the curing materials, generating $MgAl_2O_4$ crystals that were observed on the surface. This result corresponded with the study by Johnson et al. [20] and Osada et al. [15].

The results obtained for the linear shrinkage of the specimens of all formulations are presented in Table IV. Linear shrinkage was related to the loss of water and decomposition of additives (binder) and the rearrangement of particles during drying and sintering. It was possible to notice a reduction in shrinkage with an increase in the silicon carbide content and a decrease in the alumina content. This reduction was expected, due to the chemical inertness and hardness of the silicon carbide particles, which would promote the anchoring effect, causing a decrease in the size of the alumina particles [29]. Figs. 6a and 6b show the apparent porosity and water absorption, respectively, of sintered samples. There was a small increase in porosity for formulation A1, but this increase may be within the error. For the A2 formulation, it was possible to notice that with the healing there was a decrease in the apparent porosity in relation to the sintered sample. The lower porosity value for the indented samples may be an indication that, during the pressing process, there may be a variation in the packing of the particles present in the material. Comparing the values obtained for the A1 and A2 formulation test specimens, it was possible to infer that the apparent porosity increased with the increase of the silicon carbide content. This increase may be related to a decomposition of SiO_2 formed during the healing process and even during a sintering step of the specimens, as shown by Johnson et al. [20]. Comparing the healed samples, it was possible to infer that there was a small increase in the water absorption content with the increase in the silicon carbide content according to A1 and A2 formulations. The results indicated that it was not possible to state that the healing process occurred, but the values indicated that the formation of cracks or superficial microcracks during the indentation process probably did not occur.

Fig. 7 shows the surface of fractured specimens for each formulation. It was possible to see that both formulations were composed of a homogeneous surface (good mix). The results of bending strength (modulus of rupture) for the ceramic samples can be observed in Fig. 8. Fig. 9 shows the percentages of healing in relation to the indented specimens from the bending strength values for formulations A1 and A2. For the A1 formulation, it was possible to notice that there was a reduction of about 6.8% and an increase of 16.3% and 84.9% in the flexural strength of the specimens healed for 1, 30, and 60 min, respectively, in relation to the indented specimens. On the other hand, when comparing the sintered specimens with the indented specimens and those healed for 1, 30, and 60 min, there was a reduction in the strength of the specimens (about 47.3% for the indented samples and 60.9%, 38.7%, and 2.6% of the initial strength, respectively). These results showed that the increase in strength was an indication that the material presented the self-healing property, but there was a sharp drop in flexural strength for the 1 min healing time. For the A2 formulation, it was possible to notice that there was a decrease of about 11.1% and an increase of 61.1% and 48.9% in the flexural strength of the healed specimens by 1, 30, and 60 min, respectively, in relation to the indented specimens. On the other hand, when comparing the sintered specimens with the indented specimens and those healed for 1, 30, and 60 min, there was a reduction in the strength of the specimens (approximately 37.9% for the indented samples and 44.8%, 0, and 7.6% of the initial strength, respectively). Analyzing Fig. 9, it is possible to observe that for formulation A1, the increase in healing time directly influenced the percentage of healing of specimens in 1 min. The healed specimens for 60 min were the ones with the best results. For the A2 formulation, it was possible to infer from the curve that the increase in healing time directly influenced the percentage of healing of specimens after 1 min and decreased after 30 min. The healed specimens for 30 min were the ones with the best results. These results supported the hypothesis that the material produced had the ability to self-heal.

The measurement results of the reduction rate of discontinuity obtained for specimens with a healing time of 1, 30, and 60 min when heated to 1000 ºC are shown in

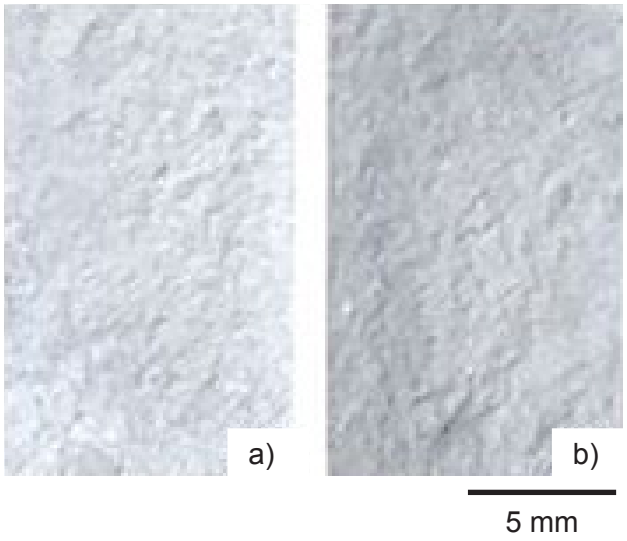

Figure 7: Images of the fractured surface of specimens of formulation: a) A1; and b) A2.

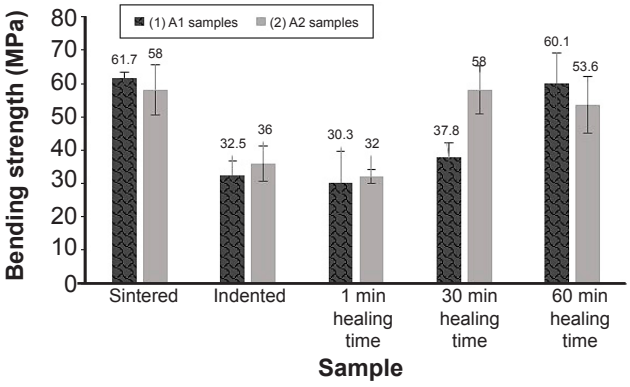

Figure 8: Flexural strength values obtained from samples A1 and A2.

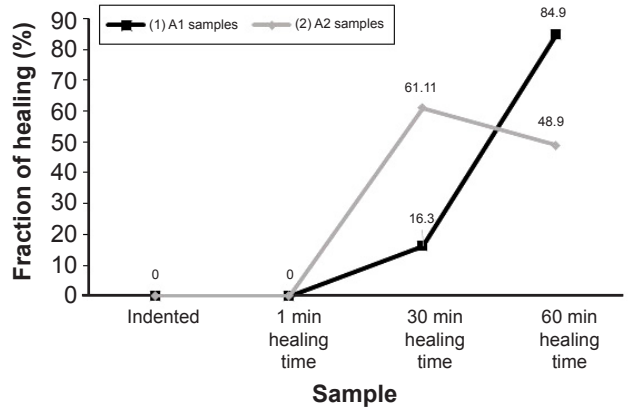

Figure 9: Values of the fraction of healing obtained for samples A1 and A2.

Table V. The indented samples were observed and measured under an optical microscope before and after healing. It was possible to see that for formulation A1, there was a reduction in all healed samples, reaching a maximum value of 19.1% within 30 min. As for formulation A2, there was also a reduction in all healed samples, reaching a maximum value of 14.8% within 30 min. These results were in line with that presented by Ando et al. [13]. The difference in discontinuities in the specimens is shown in Fig. 10. The results obtained by the reduction of discontinuity size were also indications that the material had the ability to self-heal.

Table V - Measures of reduction rate of discontinuity in the specimens after different healing times.

Sample	1 min	30 min	60 min
A1	15.9%	19.1%	15.6%
A2	9.9%	14.8%	10.0%

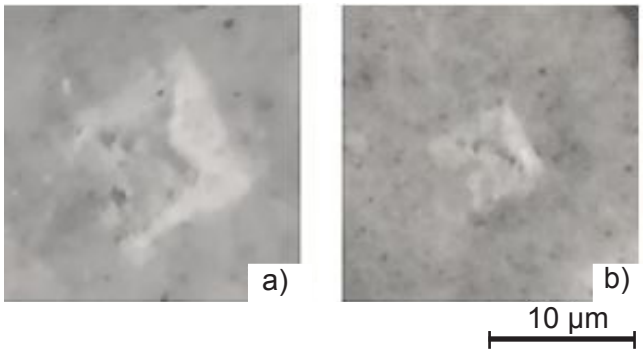

Figure 10: Micrographs of the A2 formulation sample: a) before healing; and b) after 30 min of healing time.

CONCLUSIONS

The alumina matrix composite with different contents of SiC as a healing agent and 3% MgO as a healing activator was investigated. The specimens were formed by uniaxial cold pressing and successfully sintered at 1400 ºC. It was possible to notice a reduction in linear shrinkage with an increase in the silicon carbide content and a decrease in the alumina content. Comparing the values obtained for the A1 (15% SiC) and A2 (20% SiC) formulation test specimens, it was possible to infer that the apparent porosity and water absorption increased with increasing silicon carbide content. The bending test of samples showed that the flexural strength increased by 84.9% for the A1 sample healed for 60 min and 61.1% for the A2 sample healed for 30 min, both in relation to the samples with discontinuity (made by Vickers indentation). From the measurement of sample discontinuities before and after healing for 30 min, it was possible to infer that there was a reduction of about 19.1% and 14.8% in the discontinuity size for the specimens A1 and A2, respectively. The increase in flexural strength and the reduction of discontinuity were indications that the ceramic based on silicon carbide and alumina containing an activating agent (magnesium oxide), prepared with particles of micrometric granulometry and formed by cold uniaxial pressing, was capable of self-healing. This production process can allow the manufacture of an economically viable ceramic with the ability to self-heal, achieving efficient results even using large particle sizes and a simple and cheap forming method.

ACKNOWLEDGEMENTS

The authors would like to thank CEFET-MG and CAPES for their academic and financial support.

REFERENCES

[1] M.D. Hager, P. Greil, C. Leyens, S.V.D. Zwaag, U.S. Schubert, Adv. Mater. **22**, 47 (2010) 5424.
[2] D.B. Bekas, K. Tsirka, D. Baltzis, A. Paipetis, Compos. B Eng. **87** (2016) 92.
[3] S.R. White, N.R. Sottos, P.H. Geubelle, J.S. Moore, M.R. Kessler, S.R. Sriram, E.N. Brown, S. Viswanathan, Nature **409**, 6822 (2001) 794.
[4] M. Zhang, M. Rong, Sci. China Chem. **55**, 5 (2012) 648.
[5] C. Zhang, S. Qiao, K. Yan, Y. Liu, Q. Wu, D. Han, M. Li, Mater. Sci. Eng. A **528**, 7 (2011) 3073.
[6] F. Lamouroux, S. Bertrand, R. Pailler, R. Naslain, M. Cataldi, Compos. Sci. Technol. **59**, 7 (1999) 1073.
[7] M. Mitomo, T. Nishimura, M. Tsutsumi, Mater. Sci. **15**, 22 (1996) 1976.
[8] A.C. Rodrigues, R.N.F. Souza, O.F. Galisa, T.V. França, E.C. Bianchi, C.R. Foschini, Rev. Matér. **21**, 4 (2016) 1012.
[9] R. Das, C. Melchior, K. Karumbaiah, in "Advanced composite materials for aerospace engineering", S. Rana, R. Fangueiro (Eds.), Woodhead Publ., Cambridge (2016) 333.
[10] S.K. Ghosh, in "Self-healing materials fundamentals, designs strategies and applications", S.K. Ghosh (Ed.), Wiley-VCH Verlag, Weinheim (2008) 1.
[11] X. She, A.Q. Huang, O. Lucia, B. Ozpineci, IEEE Trans. Ind. Electron. **64**, 10 (2017) 8193.
[12] M. Nakamura, K. Takeo, T. Osada, S. Ozaki, Technologies **5**, 3 (2017) 40.
[13] K. Ando, B.-S. Kim, M.-C. Chu, S. Saito, K. Takahashi, Fatigue Fract. Eng. Mater. Struct. **27**, 7 (2004) 533.
[14] Z. Chlup, P. Flasar, A. Kotoji, I. Dlouhy, J. Eur. Ceram. Soc. **28**, 5 (2008) 1073.
[15] T. Osada, K. Kamoda, M. Mitome, T. Hara, T. Abe, Y. Tamagawa, W. Nakao, T. Ohmura, Sci. Rep. **7**, 1 (2017) 1.
[16] J.C. Cremaldi, B. Bhushan, Beilstein J. Nanotechnol. **9** (2018) 907.
[17] S. Shi, T. Goto, S. Cho, T. Sekino, J. Am. Ceram. Soc. **102**, 7 (2019) 4236.
[18] G. Brant, J. Mater. Technol. **1**, 14 (1999) 17.
[19] E. Akbari, M.G. Kakroudi, V. Shahedifar, H. Ghiasi, Int. J. Appl. Ceram. Technol. **17**, 2 (2019) 491.
[20] O.T. Johnson, P. Rokebrand, I. Sigalas, in Proc. World Congr. Eng., London (2014) 2.
[21] "Powder diffraction file 02 (PDF-02)", ICDD (2003).
[22] C373-88, "Test method for water absorption, bulk density, apparent porosity and apparent specific gravity of fired whiteware products", ASTM (2006).
[23] NBR 13818, "Ceramic tiles: specification and methods of test", ABNT, Rio Janeiro (1997).
[24] A. Hamkongkaeo, W. Klysubun, T. Boonchuduang, W. Sailuam, P. Sriwattana, T. Phetrattanarangsi, K. Srimongkon, B. Sakkomolsri, A. Pimsawat, S. Daengsakul, J. Magn. Magn. Mater. **460** (2018) 327.
[25] A. Malki, Z. Mekhalif, S. Detriche, G. Fonder, A. Boumaza, A. Djelloul, J. Solid State Chem. **215** (2014) 8.
[26] M.S.R. Sarker, M.Z. Alam, M.R. Qadir, M.A. Gafur, M. Moniruzzaman, Int. J. Miner. Metall. Mater. **22**, 4 (2015) 429.
[27] A. Ortiz, F. Sánchez-Bajo, F. Cumbrera, F. Guiberteau, J. Mater. Lett. **49**, 2 (2001) 137.
[28] J. Zhou, W. Wang, Y. Cheng, Z. Zhang, Integr. Ferroelectr. **137**, 1 (2012) 18.
[29] K.P.S. Tonello, A.H.A. Bressiani, J.C. Bressiani, in Proc. Congr. Bras. Eng. Ciên. Mater., S. Paulo (2010) 19.
(Rec. 15/06/2021, Rev. 08/10/2021, 02/01/2022, Ac. 10/01/2022)